Nonlinear regime for enhanced performance of an Aharonov–Bohm heat engine ⒡

Géraldine Haack ⓘ ; Francesco Giazotto ⓘ

Check for updates

View Online

Export Citation

Nonlinear regime for enhanced performance of an Aharonov–Bohm heat engine ⓕ

View Online   Export Citation   CrossMark

Géraldine Haack[1,a)] ⓘⅅ and Francesco Giazotto[2,a)] ⓘⅅ

AFFILIATIONS

[1]Department of Applied Physics, University of Geneva, 1211 Genève, Switzerland
[2]NEST, Instituto Nanoscienze-CNR and Scuola Normale Superiore, I-56127 Pisa, Italy

Note: This paper is a part of the Special Topic Collection on Quantum Thermodynamics.
[a)]Electronic addresses: geraldine.haack@unige.ch and francesco.giazotto@sns.it

ABSTRACT

Thermal transport and quantum thermodynamics at the nanoscale are nowadays garnering increasing attention, in particular, in the context of quantum technologies. Experiments relevant for quantum technology are expected to be performed in the nonlinear regime. In this work, we build on previous results derived in the linear response regime for the performance of an Aharonov–Bohm (AB) interferometer operated as a heat engine. In the nonlinear regime, we demonstrate the tunability, large efficiency, and thermopower that this mesoscopic quantum machine can achieve, confirming the exciting perspectives that this AB ring offers for developing efficient thermal machines in the fully quantum regime.

TABLE OF CONTENTS

I. INTRODUCTION

Thermoelectricity in quantum system is nowadays gaining increasing interest since the enormous advances achieved in quantum technology. In this context, a crucial question is related to determine if the performances of thermoelectric heat engines are affected by quantum mechanics, in particular, by influencing their output power and thermodynamic conversion efficiency, especially in the nonlinear response regime.[1–7] Yet, it is well established that phase coherence and quantum effects do play a stark role in governing the overall behavior of mesoscopic heat engines.[8–13] An emblematic example of phase-tunable quantum device is represented by the celebrated Aharonov–Bohm (AB) interferometer,[14–16] where the charge particle response can be influenced by either electric or magnetic potentials. AB-type interferometers represent suitable building blocks for the implementation of efficient and versatile phase-coherent quantum heat engines. In particular, in a previous work, Ref. 13, the authors investigated the performance of AB-based quantum heat engines operated in the linear-response regime, highlighting the excellent tunability and behavior provided by magnetic fields and gate voltage control. However, experiments relevant for quantum technology applications often require the operation of a device well beyond the linear-response regime.

Here, we build upon previous results derived in the linear-response regime by investigating the behavior of an AB interferometer operated in the full nonlinear regime as a quantum heat engine. We will demonstrate the good tunability intrinsic to the device, the sizable thermodynamic conversion efficiency, and the very large thermopower that this phase-controllable thermoelectric quantum machine can achieve. All this confirms the AB interferometer as a prototypical

tool to develop efficient thermoelectric machines operating in the fully quantum regime.

After briefly recalling the model in Sec. II, this contribution is organized as follows. In Sec. III, we estimate, within a scattering-matrix approach, the thermoelectric properties of the AB ring in the nonlinear response regime, through the thermovoltage and differential Seebeck coefficient. This is done in an open-circuit configuration, as a function of the AB magnetic flux, external gate voltage, and temperature bias. We also discuss the relevance of our analysis with respect to the possible role of interactions in this device. In Sec. IV, we turn to the closed-circuit configuration that allows us to operate the AB ring setup as a heat engine. Specifically, we provide pedagogical steps toward the characterization of a quantum thermal machine in the nonlinear response regime. In Sec. V, we compute the heat current, power, and efficiency and determine the optimal load resistance for a given temperature bias in order to maximize both power and efficiency of the AB heat engine. We conclude with perspectives toward efficient phase-coherent quantum thermal machines.

II. MODEL

We start by introducing our model for the AB ring shown in Fig. 1. The AB ring is connected to two metallic contacts that can be biased in voltage or in temperature. Transmission probabilities between the contacts and the ring can be tuned for both contacts independently by controlling the transmission probability of the T-junctions.[15]
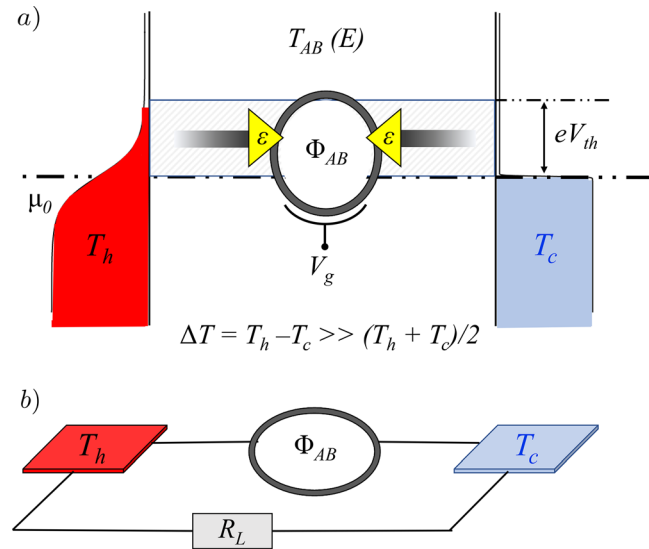

FIG. 1. Panel (a): open-circuit configuration of the AB ring in the nonlinear response regime. Left and right contacts are biased in temperatures, respectively, at T_h and T_c, and set to same chemical potential μ_0. The transmission probability of the AB ring $T_{AB}(E)$ is energy-dependent and also depends on the length (time) imbalance between the two arms: on V_g, an external gate voltage, on the transmission parameter ϵ of the T-junctions, and on Φ_{AB}, the magnetic flux piercing the interferometer. Due to thermoelectric properties of the AB ring, a thermovoltage V_{th} (eV_{th} being the corresponding energy with e the electrical charge) is developed between the contacts, in response to the temperature gradient. Panel (b): closed-circuit configuration for operating the AB ring as a quantum heat engine, when the interferometer is connected to a generic load resistor R_L through dissipationless superconducting lines.

Electrons traveling through the ring acquire two fundamentally different phase factors. One is of dynamical origin, it depends on the energy-dependent wave vector $k(E)$ of the electrons and on the length asymmetry between the two arms, whereas the other one is a geometrical phase arising from the presence of a perpendicular magnetic field to the sample, giving rise to a magnetic flux threading the ring Φ_{AB}. The momentum $k(E)$ can be controlled by an external gate voltage V_g, whereas the magnetic flux Φ_{AB} is controlled by an external magnetic field B. The total transmission probability as a function of these parameters was derived in Ref. 13, and optimal parameters' ranges were estimated. In this work, we focus on two key parameters, the external gate voltage V_g and the magnetic flux Φ_{AB}, and fix the other parameters based on Ref. 13. We recall below the energy-dependent expression of the AB ring transmission probability $T_{AB}(E)$, highlighting its dependence on V_g and on the AB flux normalized by the flux quantum $\Phi_0 = h/e$, $\varphi \equiv 2\pi\Phi_{AB}/\Phi_0$,

$$T_{AB}(E, V_g, \varphi) = \frac{f_1(E, V_g) + f_2(E, V_g)\cos\varphi}{1 + \left[f_3(E, V_g) - f_4(E, V_g)\cos\varphi\right]^2}. \quad (1)$$

The exact expressions for the functions f_i, $i = 1, \ldots, 4$ are provided in Appendix A. In Ref. 13, the functioning of this device was investigated in the linear response regime to a temperature bias across the AB ring, $\Delta T = T_h - T_c$. The linear response regime is valid when $\Delta T \ll (T_h + T_c)/2$ and amounts to neglect higher-order nonlinear terms in ΔT. The authors showed that quantum transport through the device can be fully tuned by controlling the AB flux φ. Optimal working regime for thermoelectricity in the linear response regime could be achieved with low values of ϵ, corresponding to the T-junctions behaving as two resonant tunnel barriers, similar to the Breit–Wigner regime in a Fabry–Pérot interferometer. In this following work, we extend our investigation of this fully tunable phase-coherent thermoelectric device to the nonlinear response regime, beyond small temperature bias.

III. AB THERMOELECTRICITY IN THE NONLINEAR REGIME

We start with the thermoelectric properties of the AB ring in an open-circuit configuration. Thermoelectricity refers to the ability of a device to exploit a voltage bias to induce a heat current (Peltier effect) or vice versa, to turn a temperature bias into an electrical current (Seebeck effect). Here, we focus on the latter and will characterize the behavior of the Seebeck coefficient S as a function of the AB ring's parameters. This coefficient tells us how much voltage the device is able to develop from a given temperature bias at zero charge current, $I = 0$. Because this voltage is determined at zero charge current and originates from a temperature gradient, it was named thermovoltage and will be labeled V_{th} in the following. In the linear response regime, the Seebeck coefficient S_l is simply defined as the ratio between the thermovoltage V_{th} and the small temperature difference ΔT at zero charge current,

$$S_l = \left.\frac{V_{th}}{\Delta T}\right|_{I=0}. \quad (2)$$

In general, this thermovoltage can also be built in the presence of a voltage bias V between the two contacts. In contrast, in the nonlinear response regime, it is the differential Seebeck coefficient or differential thermopower S_{nl}, which characterizes the thermoelectric response to a temperature difference ΔT (not necessarily small in this regime),

$$S_{nl} = \frac{\partial V_{th}}{\partial \Delta T}\bigg|_{I=0}. \qquad (3)$$

This definition is in full analogy with the differential resistance in the nonlinear response regime. In this work, we follow a scattering-matrix approach to compute the currents, in particular, the charge current for estimating the thermovoltage:[3,26]

$$I(V, V_g) = \frac{2e}{h}\int_{-\infty}^{\infty} dE\, T_{AB}(E, U, V_g)$$
$$\times [n(E, \mu_L, T_h) - n(E, \mu_R - eV, T_c)], \qquad (4)$$

where U describes the internal electrostatic potential of the AB ring and allows for taking into account interactions that may arise in the nonlinear response regime. Whereas U is taken at its equilibrium value U_{eq} in the linear response regime, it may depend on external potentials applied onto the sample or to the reservoirs in general. The notation $n(E, \mu_i, T_i) = (1 + e^{(E-\mu_i)/(k_B T)})^{-1}$ corresponds to the Fermi distribution of hot (left) or cold (right) contact and k_B the Boltzmann constant.

Equation (4) is valid in both linear and nonlinear response regimes. In this work, we investigate the nonlinear response regime of the AB ring, assuming no interaction, hence no change in the internal electrostatic potential, i.e., we consider it at its equilibrium value U_{eq}.[17] Within this work, we justify this assumption as follows: (i) no confined region such as a quantum dot is considered in our model, such that we avoid the Coulomb interaction in this case[18,19] and (ii) possible small modifications in U can probably be compensated through the external gate voltage V_g that we consider. We propose in this work to not consider explicitly the effect of interactions, hence to assume $T_{AB}(E, V_g)$ as given by Eq. (1) and $\mu_L = \mu_0$ and $\mu_R = \mu_0 + eV_{th}$ in the steady-state regime. Both contacts are initially set to the same chemical potential μ_0, and we have to account for V_{th} in the steady state. A gauge invariant form of Eq. (4) is then

$$I(V, V_g) = \frac{2e}{h}\int_{-\infty}^{\infty} dE\, T_{AB}(E, V_g)[n(E, \mu_0, T_h) - n(E, \mu_0 - eV, T_c)]. \qquad (5)$$

A full derivation of higher order correction terms for the thermoelectric response is left for future investigation and could be conducted following Refs. 20 and 21.

Let us now return to the thermovoltage developed through this AB ring, in response to a temperature bias. By definition, V_{th} is the solution of

$$I(V_{th}, V_g) = 0, \qquad (6)$$

with the current given by Eq. (5). The thermovoltage V_{th} corresponds to the crossing points of the I–V curves with the x-axis in Fig. 2. Here, the I–V curve shows the steady-state charge current in response to a temperature bias as a function of the voltage V for three different gate voltages V_g (solid, dashed, and dashed-dotted curves). We have fixed the magnetic flux $\varphi = \pi$ as well as the temperature bias across the sample, $T_h = 2$ K and $T_c = 0.05$ K. It can already be seen that the external voltage V_g provides an important tunability for controlling V_{th}. To further explore the thermoelectric response of the AB ring in the nonlinear regime, we show in Fig. 3 the thermovoltage as a function of the gate voltage and magnetic flux [panel (a)], and as a function of the temperature bias [panel (b) as a function of T_h, T_c being fixed]. The main features to retain from these figures are the high tunability
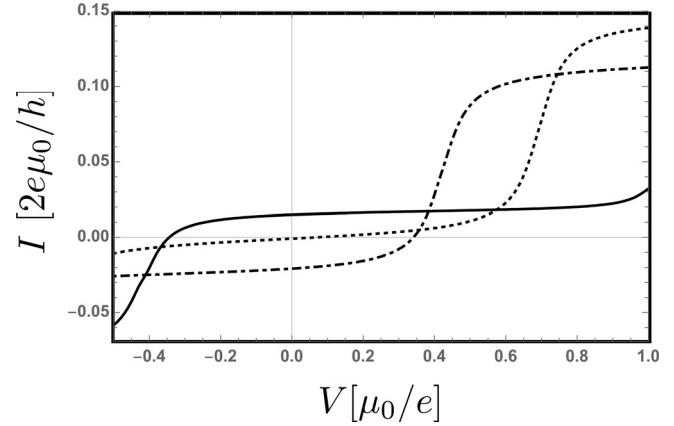

FIG. 2. I–V characteristics in the nonlinear regime for $T_h = 2$ K; $T_c = 0.05$ K, $\varphi = 2\pi\Phi_{AB}/\Phi_0 = \pi$, $\mu_0 = 10^{-22}$ J, $\varepsilon = 0.1$, and $\delta\tau = 0.3$. The curves correspond to $V_g = 0.63$ mV (solid), $V_g = 1.1$ mV (dashed), and $V_g = 1.5$ mV (dash-dotted). Thermovoltages for different V_g correspond to the crossing points with the x-axis, i.e., for $I = 0$.

of the thermovoltage with all parameters of the AB ring, and the possibility to switch on and off the thermoelectric response of the AB ring with the magnetic flux [see panel (a)].

In Fig. 3 [panel (c)], we show the differential Seebeck coefficient, see Eq. (3). Remarkably, the differential Seebeck coefficient can be two orders of magnitude larger than the one in the linear response regime: the maximum of the blue curve reaches 15 mV/K, whereas the maximum attainable in the linear response regime was of the order of 300 μV/K.[13] This confirms the excellent thermoelectric response of this phase-coherent mesoscopic device and motivates the rest of this contribution where we investigate its behavior as a quantum heat engine in a closed-circuit configuration.

IV. AB THERMOELECTRICITY IN A CLOSED-CIRCUIT CONFIGURATION

The closed-circuit configuration requires additional careful analysis for assessing correctly the thermovoltage and heat and charge currents. When the circuit is closed with a load resistance as shown in Fig. 1 [panel (b)], the Kirchhoff's laws have to be satisfied, ensuring charge and energy conservation: the sum of the charge currents flowing through the two branches of the circuit, one with the AB ring and the other one with the load resistance R_L, has to be equal to 0. As a consequence, the thermovoltage in this new configuration is obtained by solving a different equation as compared to Eqs. (5) and (6), which reads

$$\frac{2e}{h}\int_{-\infty}^{\infty} dE\, T_{AB}(E)\left[n(E, T_h) - n(E + eV_{th}^{(cl)}, T_c)\right] = -\frac{V_{th}^{(cl)}}{R_L}, \qquad (7)$$

and its solution for the thermovoltage is denoted $V_{th}^{(cl)}$ for clarity. We compute numerically values for the thermovoltages in the closed-circuit configuration as a function of gate voltage V_g and magnetic flux φ, for fixed temperatures, fixed imbalance, and fixed transmission probabilities of the T-junctions. This allows us to compute the heat current flowing through the AB ring in the nonlinear response regime according to Refs. 1, 7, and 26. Let us precise that in the context of the AB ring operated as heat engine, we have to consider the heat current
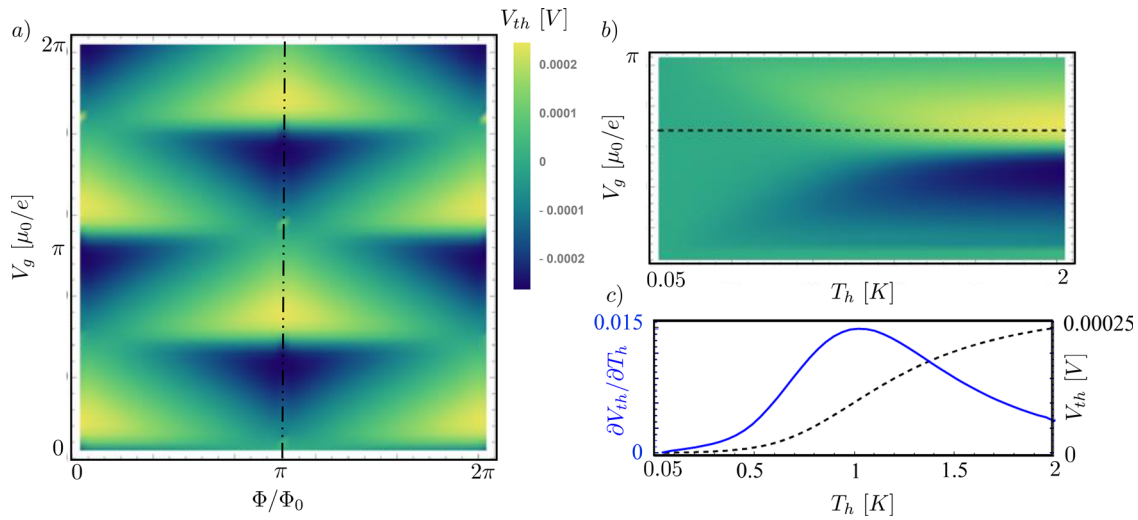
FIG. 3. Thermoelectric characteristics of the AB ring in the open-circuit configuration. Panel (a): color plot of the thermovoltage V_{th} developed across the AB interferometer vs magnetic flux $\varphi/2\pi$ and gate voltage V_g calculated for $T_c = 0.05\,\text{K}$, $T_h = 2\,\text{K}$, $\epsilon = 0.1$, and $\delta\tau = 0.3$. Numerical result with steps of $2\pi/50$ for both parameters. Panel (b): color plot of thermovoltage V_{th} as a function of the hot temperature T_h and V_g, calculated at $\varphi = \pi$ and for fixed $T_c = 0.05\,\text{K}$. Dashed line indicates a cut at $V_g = 1.26\,\text{mV}$. Panel (c): differential thermopower (Seebeck coefficient in the nonlinear regime), shown in blue solid curve with scales on the left vertical axis. It is calculated along the thermovoltage cut indicated as a dashed black curve in panels (b) and (c), left vertical axis.

flowing into the hot contact, J_h, as it corresponds to the resource for the engine.[3] It corresponds to the energy flow that electrons can dissipate into the hot reservoir, taking as reference the chemical potential of that same reservoir, here μ_0,

$$J_h = \frac{2}{h} \int_{-\infty}^{\infty} dE (E - \mu_0) T_{AB}(E) \left[n(E, T_h) - n\left(E + eV_{th}^{(cl)}, T_c\right) \right]. \quad (8)$$

For clarity, we recall that heat current is not conserved, $J_h \neq J_c$ with J_c the heat current flowing into the cold contact. In the case of the AB ring operated as heat engine with the building up of a thermovoltage on the right (cold) lead, conservation law instead reads

$$J_h + J_c = V_{th}^{(cl)} I, \quad (9)$$

with

$$J_c = \frac{2}{h} \int_{-\infty}^{\infty} dE (E - (\mu_0 - eV_{th}^{(cl)}) T_{AB}(E) \left[n(E + eV_{th}^{(cl)}, T_c) - n(E, T_h) \right]. \quad (10)$$

We also compute the power $P = (V_{th}^{(cl)})^2/R_L$ generated by the AB heat engine, which allows us in Sec. V to discuss several figures of merit for the AB heat engine in the nonlinear response regime. The load resistance is typically expressed as a multiple of the quantum of resistance $R_q = h/(2e^2)$. The numerical integration over energy for computing the heat current was performed over ten times the Fermi energy μ_0. Let us remark that it takes values of the same order of magnitude as the one in the linear response regime for $T = 1\,\text{K}$, namely, of the order of 0.1–1 pW, see Appendix B. Figure 4 [panel (a)] shows the power for a fixed value of the load resistance, $R_L = 20\,R_q$ as a function of gate voltage and magnetic flux, and panel (b) highlights the power characteristics for different gate voltages as a function of the magnetic

flux. The cuts evidence the possibility to fully turn on and off the heat engine, from 0 to maximal power.

V. POWER AND EFFICIENCY OF THE AB HEAT ENGINE IN THE NONLINEAR RESPONSE REGIME

We now investigate the power versus efficiency trade-off in the nonlinear regime, as a function of the gate voltage V_g and the load resistance R_L. Given a temperature bias, we determine the optimal load resistance to maximize both power and efficiency, the latter being simply defined as the ratio of power (output of the engine in $[W]$) and heat current into the hot reservoir (input of the engine, also in $[W]$),

$$\eta = P/J_h. \quad (11)$$

In Fig. 4(c), we show the Lasso-type parametric plot of efficiency versus power, which evidences the trade-off between both quantities. A heat engine with maximal efficiency, Carnot efficiency, does not produce any power as it corresponds to the point of reversibility for the machine.[3] Hence, a compromise must be found or determined depending on the primary goal of the engine (to produce more power with less efficiency or be more efficient with less output power). Here, we show that the AB heat engine can be easily tuned through external gate voltage V_g [panel (c)] to optimize either efficiency or power. These two quantities also depend on the load resistance, as evidenced by the different colored curves in the same panel. For the AB heat engine, it seems that a load resistance of $R_L \sim 15$–$20\,R_q$ may be optimal, given the values we have fixed for the other parameters. Interestingly, an efficiency up to ~40% of Carnot efficiency can be achieved by adjusting V_g and R_L. This value has to be compared to the efficiency in the linear response regime for similar temperature gradient, where the authors showed a maximal efficiency of the order of 30% the Carnot efficiency.[13] The increase in efficiency can directly be
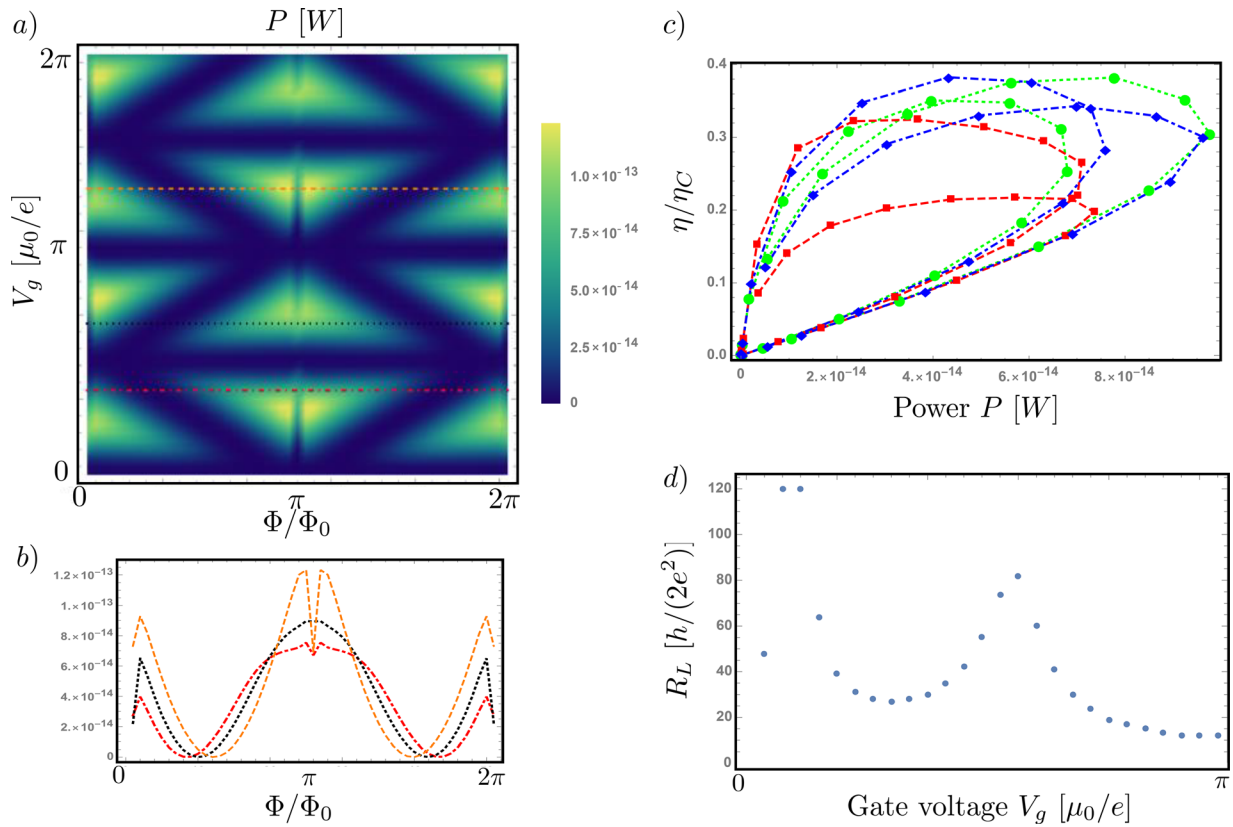
Fig. 4. Closed-circuit characteristics of the AB heat engine. Panel (a): color plot of the power $P = (V_{th}^{(cl)})^2/R_L$ as a function of gate voltage V_g and magnetic flux φ. Panel (b): cuts of power as a function of magnetic flux for different values of the gate voltage, $V_g = 0.79$ mV (red dot-dashed), $V_g = 1.4$ mV (black dotted), and $V_g = 2.7$ mV (orange dashed). Cuts are also shown on panel (a). Nonlinear behavior of power values for the other parameters for panels (a) and (b): $T_h = 2$ K, $T_c = 0.05$ K, $\varepsilon = 0.1$, $\delta\tau = 0.3$, and $R_L = 20\,R_q$. Panel (c): parametric plot of the efficiency normalized by the Carnot efficiency η_C versus power P, as a function of the gate voltage $V_g = [0, \pi(\mu_0/e)]$ in steps of $\Delta V_g = 2\pi/50(\mu_0/e)$. Different colors correspond to different load resistances: green (circles) for $R_L = 15R_q$, blue (diamonds) for $R_L = 20R_q$, and red (squares) for $R_L = 40R_q$. Values of the other parameters are the same as for panels (a) and (b) with fixed magnetic flux, $\varphi = \pi$. Panel (d): optimal load resistance as a function of V_g, for maximizing efficiency and power, see main text.

attributed to the nonlinear response of the AB engine, as similar temperature bias across the setup was considered (while keeping the same parameters for asymmetry, T-junctions parameter, and magnetic flux. In panel (d), we show the optimal load resistance to maximize both efficiency and power, as a function of the gate voltage. To achieve this, we maximize $P + \eta$, over R_L for fixed V_g and fixed temperature gradients. This procedure does not reflect the absolute optimal R_L as a function of all parameters (of interest in possible future experiments), but rather the high tunability of the AB ring as heat engine to achieve sizeable power and efficiency in the quantum regime.

VI. CONCLUSIONS AND PERSPECTIVES

In conclusion, we have analyzed a coherent mesoscopic heat engine consisting of an Aharonov–Bohm quantum interferometer operated in the full nonlinear regime. The device thermoelectric response turns out to be sizable, and the interferometer is able to provide a thermopower, which is about 50 times larger than in the same structure operated in the linear regime. Moreover, also the heat engine thermoelectric efficiency at maximum power is somewhat large,

obtaining values as high as ~40% of the Carnot efficiency in the linear regime. The AB heat engine can provide magnetic flux- and electrostatic-driven control of charge and heat current as well as of its thermoelectric response under physical conditions, which are accessible from the experimental point of view. Suitable candidates for the implementation of the Aharonov–Bohm quantum heat engine are represented by metallic or GaAs/AlGaAs two-dimensional electron gas heterostructures,[22–25] which are expected to yield devices with robust performances over a wide range of system parameters. Future experiments will also stimulate further theoretical work to address the effect of interactions that may induce corrections due to a modified internal electrostatic potential. The above results show that an Aharonov–Bohm loop operated as a quantum heat engine in the non-linear regime represents a prototypical platform for the implementation of a unique class of phase-tunable thermoelectric quantum machines operating at cryogenic temperatures. Yet, in the context of quantum technologies,[27] this coherent structure might be at the core of a number of innovative thermoelectric quantum devices, for instance, highly sensitive photon sensors, where radiation-induced
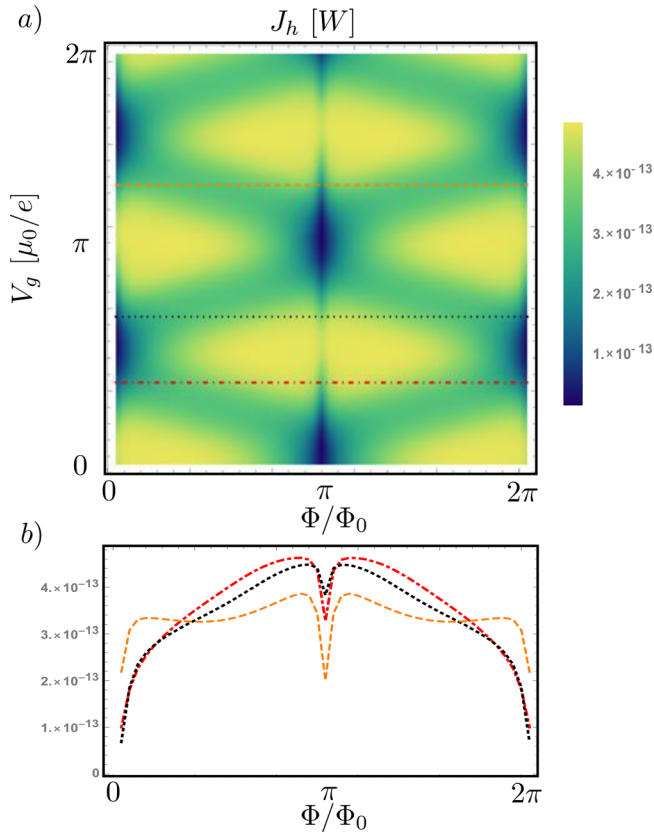
a)

b)

FIG. 5. Heat current through the AB heat engine in a closed-circuit configuration. Panel (a): color plot of the heat current J_h [see Eq. (8)], as a function of gate voltage V_g and magnetic flux φ. Panel (b): cuts of heat current as a function of magnetic flux for different values of the gate voltage, $V_g = 0.79$ mV (red dot-dashed), $V_g = 1.4$ mV (black dotted), and $V_g = 2.7$ mV (orange dashed). Other parameters are fixed: $T_h = 2$ K, $T_c = 0.05$ K, $\varepsilon = 0.1$, and $\delta\tau = 0.3$.

heating, one of the electrodes forming the system, is detected via the resulting thermovoltage.

ACKNOWLEDGMENTS

AUTHOR DECLARATIONS

Conflict of Interest

The authors have no conflicts to disclose.

DATA AVAILABILITY

The data that support the findings of this study are available within the article and from the corresponding author upon reasonable request.

APPENDIX A: TRANSMISSION PROBABILITY OF THE AB RING

In this section, we provide the expressions of the functions f_i in Eq. (1) of the transmission probability of the AB ring. These coefficients are determined and expressed according to Ref. 13, where the authors previously derived T_{AB} in full generality,

$$f_1(E, V_g) = 1 - \cos\chi \cos\delta\chi, \tag{A1}$$

$$f_2(E, V_g) = \cos\delta\chi - \cos\chi, \tag{A2}$$

$$f_3(E, V_g) = \frac{2(1-\varepsilon)\cos\chi - \left(1 - \varepsilon - \sqrt{1-2\varepsilon}\right)\cos\delta\chi}{2\varepsilon \sin\chi}, \tag{A3}$$

$$f_4(E, V_g) = \frac{\left(1 - \varepsilon + \sqrt{1-2\varepsilon}\right)}{2\varepsilon \sin\chi}, \tag{A4}$$

with $\chi = \chi_1 + \chi_2$ and $\delta\chi = \chi_1 - \chi_2$ and $\chi_i = k_i L_i$ are the dynamical phases that electrons acquire while traveling in each arm $i = 1, 2$. Here, k_i is the energy-dependent wave vector and L_i is the length of the corresponding arm,

$$k_1(E) = \tilde{k}_{\mu_0} + \frac{E - \mu_0}{\hbar v_d}, \quad k_2(E) = \tilde{k}_{\mu_0} + \frac{E - (\mu_0 + eV_g)}{\hbar v_d}. \tag{A5}$$

For an asymmetric AB ring, the difference and sum of the dynamical phases then read

$$\chi_1 + \chi_2 = (2L + \delta L)\left(\tilde{k}_{\mu_0} + \frac{E - \mu_0}{\hbar v_d}\right) - \frac{eV_g L}{\hbar v_d}, \tag{A6}$$

$$\chi_1 - \chi_2 = \delta L\left(\tilde{k}_{\mu_0} + \frac{E - \mu_0}{\hbar v_d}\right) + \frac{eV_g L}{\hbar v_d}. \tag{A7}$$

Here, we have defined $L_1 \equiv L + \delta L$, $L_2 \equiv L$, where v_d is the electronic drift velocity, and the Fermi wave vector is tuned through energy offsets applied onto each arm ($k_{\mu_0} \to \tilde{k}_{\mu_0}$).

APPENDIX B: HEAT CURRENT

For completeness, we provide with Fig. 5 a color plot of the heat current as a function of voltage gate and magnetic flux, similar to the power shown in Fig. 4 [panels (a) and (b)]. We also indicate the same cuts for values of V_g given in the main text.

REFERENCES

[1]H. van Houten, L. W. Molenkamp, C. W. J. Beenakker, and C. T. Foxon Semicond. Sci. Technol. **7**, 215 (1992).
[2]F. Giazotto, T. T. Heikkilä, A. Luukanen, A. M. Savin, and J. P. Pekola, Rev. Mod. Phys. **78**, 217 (2006).
[3]G. Benenti, G. Casati, K. Saito, and R. S. Whitney, Phys. Rep. **694**, 1–124 (2017).
[4]R. S. Whitney, R. Sanchez, and J. Splettstoesser, "Quantum thermodynamics of nanoscale thermoelectrics and electronic devices," in *Thermodynamics in the Quantum Regime* (Springer, New York, 2019).

02 August 2024 07:52:18

[5]R. S. Whitney, Phys. Rev. Lett. **112**, 130601 (2014).

[6]R. S. Whitney, Phys. Rev. B **91**, 115425 (2015).

[7]D. Sánchez and R. López, C. R. Phys. **17**, 1060 (2016).

[8]Y. M. Blanter, C. Bruder, R. Fazio, and H. Schoeller, Phys. Rev. B **55**, 4069 (1997).

[9]P. P. Hofer and B. Sothmann, Phys. Rev. B **91**, 195406 (2015).

[10]C. J. Lambert, H. Sadeghi, and Q. H. Al-Galiby, C. R. Phys. **17**, 1084 (2016).

[11]P. Samuelsson, S. Kheradsoud, and B. Sothmann, Phys. Rev. Lett. **118**, 256801 (2017).

[12]S.-Y. Hwang, F. Giazotto, and B. Sothmann, Phys. Rev. Appl. **10**, 044062 (2018).

[13]G. Haack and F. Giazotto, Phys. Rev. B **100**, 235442 (2019).

[14]Y. Aharonov and D. Bohm, Phys. Rev. **115**, 485 (1959).

[15]M. Büttiker, Y. Imry, and M. Y. Azbel, Phys. Rev. A **30**, 1982 (1984).

[16]A. Levy-Yeyati and M. Büttiker, Phys. Rev. B **52**, 14360(R) (1995).

[17]M. Büttiker and D. Sanchez, Int. J. Quantum Chem. **105**, 906 (2005).

[18]A. Yacoby, M. Heiblum, D. Mahalu, and H. Shtrikman, Phys. Rev. Lett. **74**, 4047 (1995).

[19]G. Hackenbroich and H. A. Weidenmüller, Phys. Rev. Lett. **76**, 110 (1996).

[20]D. Sánchez and R. López, Phys. Rev. Lett. **110**, 026804 (2013).

[21]A. R. Hernandez and C. H. Lewenkopf, Phys. Rev. Lett. **103**, 166801 (2009).

[22]R. A. Webb, S. Washburn, C. P. Umbach, and R. B. Laibowitz, Phys. Rev. Lett. **54**, 2696 (1985).

[23]B. S. Washburn and R. A. Webb, Adv. Phys. **35**, 375 (1986).

[24]A. Yacoby, R. Schuster, and M. Heiblum, Phys. Rev. B **53**, 9583 (1996).

[25]M. Yamamoto, S. Takada, C. Bäuerle, K. Watanabe, A. D. Wieck, and S. Tarucha, Nat. Nanotechnol. **7**, 247 (2012).

[26]G. B. Lesovik and I. A. Sadovskyy, Phys.-Usp. **54**, 1007 (2011).

[27]A. Acin *et al.*, New J. Phys. **20**, 080201 (2018).

02 August 2024 07:52:18